Cell Communication and Signaling

RESEARCH

Open Access

A ketogenic diet alleviates the apoptosis of granulosa cells by inhibiting the activation of cGAS-STING signaling pathway in PCOS mice

Bining Zhao[1,3†], Haowen Wu[1,3†], Qiyang Yao[1,3], Wenpei Bai[2*] and Jihong Kang[1,3*]

Abstract

Background Polycystic ovary syndrome (PCOS) is the most common cause of anovulatory infertility. The ketogenic diet (KD), a diet high in fat and low in carbohydrates, has been applied clinically for the treatment of obese women with PCOS. We have previously demonstrated that KD improved the reproductive phenotype in an androgen-induced PCOS mouse model, yet the underlying molecular mechanisms remain largely unclear. The aim of the present study was to investigate the effect of KD on the reproductive phenotype of a letrozole-induced PCOS mouse model.

Methods Female C57BL/6N mice were divided into three groups, designated control, letrozole, and letrozole + KD groups. Mice of control and letrozole groups were fed the control diet, whereas letrozole + KD mice were fed a KD with 89.9% (kcal) fat for 3 weeks after the PCOS mouse model was generated. β-hydroxybutyrate (BHB), the most abundant ketone body in the body, was used to treat KGN cells with testosterone (T) to simulate the KD effect on PCOS mouse ovaries in vitro.

Results Our data showed that KD treatment significantly increased blood ketone levels and reduced body weight. Ovarian functions were improved in some letrozole + KD mice. Results from in vitro experiments indicated mitochondrial damage owing to high T levels, which resulted in the leakage of cytochrome C and mitochondrial DNA into the cytosol and thus induced the activation of the intracellular caspase cascade and the cGAS-STING-NF-κB pathway, leading to granulosa cell inflammation and apoptosis. BHB exhibited certain protective effects on mitochondria of T-treated KGN cells via inhibiting the cGAS-STING pathway. Moreover, the cGAS-STING pathway was activated in ovaries of letrozole mice and was down-regulated in letrozole + KD mice.

Conclusion These findings, for the first time, revealed that hyperandrogenism induced ovarian dysfunction possibly through activation of the cGAS-STING pathway, which could be partially inhibited by ketone bodies produced from KD administration.

Keywords Polycystic ovary syndrome, Ketogenic diet, Hyperandrogenemia, Mitochondrial dysfunction, cGAS-STING pathway, Inflammation, Apoptosis

†Bining Zhao and Haowen Wu contributed equally to this work.

*Correspondence:
Wenpei Bai
baiwp@bjsjth.cn
Jihong Kang
kangjihong@bjmu.edu.cn
Full list of author information is available at the end of the article

Background

Polycystic ovary syndrome (PCOS) is one of the most common endocrinopathies affecting 10% to 13% women of reproductive age [1]. The clinical presentations of this condition include hyperandrogenism (HA), ovulatory dysfunction (OD), and polycystic ovarian morphology (PCOM), involving reproductive, metabolic, and psychological impairments [2]. Obesity is common in PCOS. The link between obesity and the prevalence of PCOS is highly correlated. For overweight or obese women with PCOS, body weight control is recommended as a fundamental strategy for the treatment. Several dietary patterns in the management of PCOS have been extensively investigated, including the low saturated-fat diet, low glycemic index (GI) diet, Mediterranean diet (MD), Pulse-Based diet, and ketogenic diet (KD) [3, 4]. Among these, the KD emerges as a possible non-pharmacological therapy in main endocrine diseases of the female reproductive system and plays a role in improving fertility outcomes, low-grade inflammation, body weight, etc.

The KD was first mentioned in the 1920s as a dietary approach for treating patients with drug-resistant epilepsies. In the classic KD, 90% of the calories come from fat, 8% from protein, and only 2% from carbohydrates [5]. The use of KD has been widely established in the treatment of neurological disorders [6]. Recently, emerging evidence suggests its potential as a viable therapeutic approach for metabolic conditions such as type 2 diabetes (T2D) and obesity [7].

Administration of the KD induces substantial ketone body production and facilitates nutritional ketosis. Ketone bodies (acetoacetate (AcAc), β-hydroxybutyrate (BHB), and acetone) are mainly produced by the hepatocyte mitochondria. BHB is the most abundant ketone body in the body, serving as not only an energy metabolism substrate but also a crucial signaling molecule in ameliorating metabolic abnormalities [8–11]. The possible mechanisms may involve inhibition of inflammation [9–11], histone β-hydroxybutyrylation (Kbhb) [12], and others.

Accumulated clinical cases have reported significant therapeutic effects of KD on women with PCOS [4, 13–15]. The underlying mechanisms, however, remain largely unknown. Previous data from our laboratory [16] have demonstrated that a classic KD administrated for one or three weeks had certain ameliorative effects on reproductive and metabolic abnormalities, especially on ovarian functions in dehydroepiandrosterone (DHEA)-induced PCOS mouse model. Moreover, BHB ameliorated inflammation and apoptosis of ovarian granulosa cells as observed from in vitro experiments. However, whether the KD also functions in other PCOS mouse models, particularly in non-exogenous-androgen-induced animal models, and the intrinsic mechanisms of improving ovarian functions need to be deeply investigated.

Therefore, letrozole was employed in the present study to induce a PCOS mouse model as reported [17] and the effects of KD on the reproductive phenotype of the mice were evaluated. Furthermore, the mechanisms were studied in KGN cells. Our results suggested an important role for mitochondria dysfunction-activated cGAS-STING signaling pathway in PCOS mouse granulosa cells and the protective effects of BHB on inflammation and apoptosis under these conditions.

Materials and methods

Animals and experimental protocols

Female C57BL/6N mice at the age of 21 days were purchased from Beijing Vital River Laboratory Animal Technology Co., Ltd. (Beijing, China). The animals were acclimated to standard laboratory conditions (22 °C ± 2 °C, 12 h light:12 h dark) with free access to rodent food and water. At postnatal day 25, the mice of comparable weights were randomly divided into three groups as illustrated in Fig. 1. Group 1: control group (ctrl). The mice ($n=18$) were fed a normal chow and received the vehicle (1% saline solution of sodium carboxymethylcellulose, 0.5 mL per 100 g body weight) once daily by oral gavage for three weeks. Group 2: Letrozole group (letro). The mice ($n=18$) were fed a normal chow and received letrozole (Sigma, USA) (0.1 mg per 100 g body weight) dissolved in 1% saline solution of sodium carboxymethylcellulose once daily by oral gavage for three weeks. Group 3: Letrozole + KD group (letro + KD). The mice ($n=12$) were fed a normal chow and received letrozole for three weeks in the same way as in Group 2. After 3 weeks of the treatments, 6 mice from control group and 6 mice from letrozole group were sacrificed to verify the establishment of the PCOS animal model. The remaining 12 control mice were fed a control diet (Moldiet, USA) (10% of calories from fat; 10% of calories from protein; 80% of calories from carbohydrates) and administered with the vehicle for another 3 weeks. The remaining letrozole mice in Group 2 were fed a control diet and administered with letrozole for 3 weeks. The letro + KD mice in Group 3 were fed a ketogenic diet (Moldiet, USA) (89.9% of calories from fat; 10% of calories from protein; 0.1% of calories from carbohydrates) and administered with letrozole for 3 weeks according to our previous work [16]. The mice were weighed daily during the treatments. In addition, the energy intake of the mice was recorded every day. The amount of energy intake of the letro + KD mice was strictly controlled according to the amount of the energy intake of the letro mice the day before and did not exceed the average

energy intake of the letro mice. After 3 weeks of feeding with a KD or a control diet, all the mice in the three groups were sacrificed. The animal experiments were approved by Institutional Animal Care and Use Committee (IACUC) of Peking University Health Science Center accordance with the Guide for the Care and Use of Laboratory Animals published by the US National Institutes of Health.

Blood ketone measurement

Blood ketone levels were measured three times during the treatments, namely one day before the feeding of the KD, once during the second week and once during the third week of the KD feeding. Blood samples were collected from the tail vein and blood ketone levels were immediately measured with the blood ketone monitoring system (Abbott, USA).

Estrous cycle determination

The estrous cycle was determined daily 5 weeks after the treatments and assessed for 7 consecutive days. As described previously [18], vaginal cells were collected via saline lavage and stained with methylene blue (0.1%). Cells were then observed under the microscope and the stages of the estrous cycle were determined based on vaginal cytology: predominant leukocytes indicated the diestrus stage, predominant nucleated epithelial cells indicated the proestrus stage, predominant cornified squamous epithelial cells indicated the estrus stage, and both cornified squamous epithelial cells and leukocytes indicated the metestrus stage.

Tissue collection and histology

The animals were anesthetized by intraperitoneal injection of a mixture containing ketamine hydrochloride (100 mg/kg) and xylazine (20 mg/kg). Blood samples were collected through the angular vein of the mice. Ovary tissues were rapidly removed from the animals. One ovary from each mouse was fixed in 4% paraformaldehyde (PFA) and postfixed in a 20% sucrose solution. Afterward, tissues were embedded in paraffin. The other ovary was snap frozen in liquid nitrogen and stored at -80℃ for subsequent RNA extraction. To examine ovarian morphology, ovary tissues were cut into sections (7-μm thickness). Every 10th wax section was mounted on a glass slide. The sections were stained with hematoxylin and eosin (H&E) (Biosharp, China) according to the standard histological procedures. Numbers of cystic follicles, corpora luteum, and follicles at all stages were counted. The areas of ovarian cysts were also measured with ImageJ (National Institutes of Health) software.

Immunohistochemistry and H-score analysis

Immunohistochemistry was performed as described previously [18]. In brief, ovarian sections were deparaffinized and washed. Endogenous peroxidase activity was quenched with endogenous peroxidase blocking regent (ZSGB-BIO, China). Antigen retrieval was performed by heating sections in 0.1 mM citrate (pH 6.0) for 30 min at 98 °C. Tissue sections were then blocked with 1% bovine serum albumin for 20 min at 37 °C, followed by overnight incubation at 4 °C with rabbit anti-cGAS (Proteintech, China) or rabbit anti-STING (Abclonal, China) monoclonal antibodies. Nonimmune immunoglobulin G (IgG) was used as the negative control. Sections were then incubated with a peroxidase-labeled secondary antibody (ZSGB-BIO, China). Immunostaining was revealed by using diaminobenzidine and counterstained with hematoxylin. For each section stained, three high-power fields (400×) were randomly selected for analysis.

Immunoreactivity in specimens was quantified by the H-score system, which was a widely used semi-quantitative method that described staining intensity and distribution. The relative intensity of specific staining was defined as negative (0), low positive (1+), positive (2+) and high positive (3+). The final score was the sum of

(See figure on next page.)

Fig. 1 KD improves the ovarian function and reduces apoptosis and inflammation in the ovaries of letrozole-induced PCOS mice. **A** The experimental flow chart of generating letrozole-induced PCOS mice and the following KD/control diet treatments. **B** Serum ketone levels in three groups of mice after modeling and during the second and third weeks of the KD/control diet treatments. $n=6$ per group. **C** Body weight curves of the mice during the experiments. $n=6$ per group. The shaded area shows the period during which the mice were treated with a control diet or KD. $n=6$ per group. **D** Final body weight of the three groups of mice after treatment with control diet or KD for 3 weeks. $n=6$ per group. **E** Serum testosterone (T) levels in mice at the end of the experiment. $n=6$ per group. **F** Representative estrous cycle of one mouse from each group. D, diestrus; M, metestrus; E, estrus; P, proestrus. **G** Representative H&E staining of ovarian sections of one mouse from each group. The yellow arrows indicate corpora luteum and the blue arrows indicate ovarian cysts. Micrographs were taken at magnifications × 50, scale bar = 100 μm. **H** The number of ovary cysts, corpora luteum, and follicles at all stages of the mice after treatment with a control diet or KD for 3 weeks. $n=6$ per group. **I** The percentage of cysts' area of the mice treated with a control diet or KD for 3 weeks. $n=6$ per group. **J** Representative TUNEL staining of ovarian sections of one mouse from each group. Micrographs of bright field (BF) were taken at magnification × 100. **K** The relative mRNA expression of IL-6 in the ovaries of the mice treated with a control diet or KD for 3 weeks. $n=6$ per group. **L** The relative levels of IL-6 in the ovarian supernatants of the mice treated with a control diet or KD for 3 weeks were detected by ELISA. $n=6$ per group. Data are presented as mean ± SEM. *, $P<0.05$ *vs* ctrl, **, $P<0.01$ *vs* ctrl, #, $P<0.05$, ##, $P<0.01$. KD: ketogenic diet

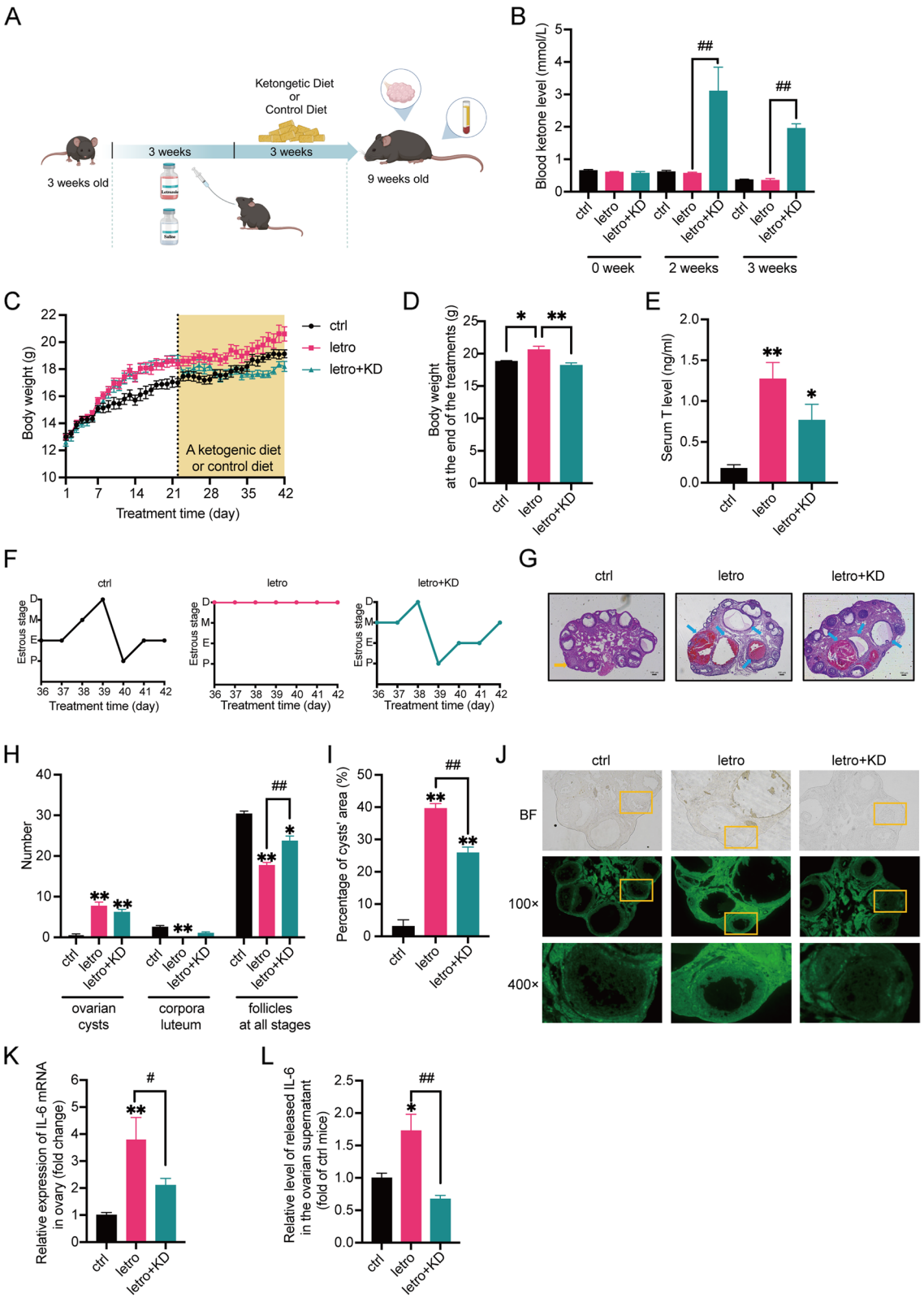

Fig. 1 (See legend on previous page.)

the relative intensity of specific staining multiplied by the percentage of positive cells [19]. The H-score scale ranged from 0 to 300. Both data were obtained by ImageJ (National Institutes of Health) software analysis.

TUNEL staining

The apoptosis of the ovarian tissues from the mice was detected by terminal deoxynucleotidyl transferase-mediated dUTP nick-end labeling (TUNEL) staining with a commercially available kit from Elabscience Biotechnology Co., Ltd according to the manufacturer's instructions. Fluorescence was visualized using a fluorescence microscope (Olympus, Japan) and images were captured using FCSnap software.

Measurement of interleukin-6 (IL-6) levels by ELISA

IL-6 in the culture medium was measured by using ELISA kit (ABclonal, China) according to the manufacturer's instructions. For the detection of IL-6 in the ovaries, ovarian supernatants were extracted as described previously [20]. Briefly, 20 μL of saline was added to each ovary sample. Ovaries were then punched with microsurgical scissors to release ovarian supernatant. After centrifugation at 12,000 rpm at 4 °C for 10 min, the supernatants were collected. Then IL-6 levels in the ovarian supernatants were detected with ELISA kit.

Cell culture and treatments

KGN cells, a human ovarian granulosa cell line, were purchased from Beijing Aitemeng Science and Technology Co (catalog number: BNCC-337610). The cells were cultured in Dulbecco's Modified Eagle's Medium (DMEM) supplemented with 4500 mg/l glucose, 10% fetal bovine serum (FBS), and 100 U/mL penicillin/streptomycin at 37 °C in a humidified 5% CO2 atmosphere in air. The medium was changed every 2 days. After confluence, cells were pre-treated with BHB at 5 mM for 6 h, followed by the treatment with a combination of BHB and testosterone (T) (10 μM) for 24 h according to our previous work [16]. Cells were recovered for protein assay or interleukin-6 (IL-6) determination.

Analysis of cell viability with the MTT assay

KGN cells were cultured in a 96-well plate. After reaching a confluence of approximately 90%, the culture medium was removed and the prepared MTT (Solarbio, China) working solution was added to each well. The plate was incubated for 4 h at 37 °C followed by the addition of dimethyl sulfoxide (DMSO) to solubilize the formazan produced. The absorbance was read at 490 nm using a microplate reader.

Detection of cell apoptosis by flow cytometry

KGN cells were collected from 6-well plates by trypsin without EDTA. Cells were harvested and resuspended in Annexin V binding buffer containing AnnexinV-FITC and propidium iodide (PI) (Elabscience, China) according to the manufacturer's instructions. Samples were then incubated for 10 min at room temperature in the dark. Flow cytometry data were acquired on Guava® easyCyte™ (Luminex, USA).

Real-time PCR analysis

Total RNA from cells or tissues was extracted by using the TRIzol as described previously [21]. Aliquots of 1 μg of total RNA from each sample were reverse transcribed to cDNA with a reverse transcription kit (Vazyme, China). Primer sequences were listed in the Supplemental Table 1. Real-time PCR was performed using fluorescent SYBR Green PCR Master Mix (Vazyme, China) according to the manufacturer's instructions (Agilent Technologies, USA). β-actin was used as an internal standard. The expression of the target gene was normalized to that of β-actin within the same sample using the $2^{-\triangle\triangle Ct}$ method. Each sample was measured in duplicate in each experiment.

Western blot analysis

Western blot analysis was performed as described previously [21]. Briefly, aliquots of 20 μg of protein from each sample were separated on 10–12% SDS-PAGE and then transferred to a nitrocellulose (NC) membrane. The membrane was blocked with 5% skimmed milk and subsequently probed with primary antibodies at 4 °C overnight. β-actin was used as an internal control. The membrane was washed with TBST buffer and then incubated with a horseradish peroxidase-conjugated secondary antibody. After washing, the membrane was developed with ECL Reagent (Tanon, China). Blots were detected with chemiluminescence (Tanon, China). Protein expression levels were quantified using Image J software.

Detection of ROS by DCFH-DA

Intracellular reactive oxygen species (ROS) were detected using the DCFH-DA fluorescence probe (Solarbio, China) according to the manufacturer's instructions. Briefly, KGN cells were washed with PBS

and then incubated with DCFH-DA staining working solution for 20 min at 37 °C. After that, the solution was removed and cells were washed twice with PBS. The fluorescence of the cells was detected immediately using a fluorescence microscope (Leica, Germany).

Determination of mitochondrial membrane potential

Mitochondrial membrane potential of KGN cells was detected with mitochondrial membrane potential assay kit with JC-1 (Beyotime, China) according to the manufacturer's instructions. Briefly, KGN cells were washed twice with PBS and then incubated with JC-1 working solution for 20 min at 37 °C. The staining solution was removed and cells were washed twice with buffer solution. The fluorescence of the cells was monitored immediately using a fluorescence microscope (Leica, Germany).

Extraction and quantification of mitochondrial DNA (mtDNA)

The mtDNA was extracted from cells as reported previously [22]. In brief, KGN cells were lysed in 170 μL of digitonin lysing buffer (150 mM NaCl, 50 mM HEPES pH 7.4, 2.5 μg/mL digitonin) at 4 °C for 10 min, followed by centrifugation at 20000 × g at 4 °C for 20 min. The DNA extraction kit (Vazyme, China) was used to separate the DNA components from the lysate. The supernatant that was enriched with cytoplasmic mtDNA was collected and quantified using real-time PCR.

Small interfering RNA (siRNA) transfection

Three siRNAs containing sequences targeting the mouse *cGAS* mRNA and one non-silencing RNA as negative control (nc) were obtained from AZENTA Life Science, China. The sequences were listed in the Supplemental Table 2. Transfection of siRNA was performed as described previously [21]. In brief, when KGN cells reached the confluence of 70–80%, the culture medium was replaced with DMEM without serum or antibiotics. The siRNAs or non-silencing RNA (nc) diluted in the transfection medium were transfected into KGN cells using the transfection reagent Lipofectamine 3000 (ThermoFisher, USA) according to the manufacturer's instructions. The cells were kept in the transfection medium for 12 h. Then the siRNA-containing medium was changed to DMEM with 10% FBS and 100 U/mL penicillin/streptomycin. Thirty-six hours after transfection, cells were harvested for RNA extraction to validate transfection efficiency. Forty-eight hours after transfection, the cells were either harvested for protein extraction to validate the transfection efficiency or were utilized for other experiments.

Statistical analysis

Data are presented as mean ± standard error of the mean (SEM). Statistical analyses were performed with GraphPad Prism 9.4.0 software. Data for comparisons were analyzed by one-way ANOVA followed by Bonferroni posttest. $P < 0.05$ was considered statistically significant.

Result

KD increases serum ketone levels and reduces body weight and blood glucose levels

The letrozole-induced PCOS mice were generated as reported before [17]. The establishment of this model was confirmed by elevated serum testosterone levels, disturbed estrous cycles, and the presence of large antral follicles (diameter > 311 μm) (Supplemental Figs. 1A-C). After three weeks of treatments, mice of ctrl and letro groups received continuous administration of saline or letrozole, respectively, and were both fed the control diet for three weeks. Mice of the letro + KD group received continuous administration of letrozole by oral gavage to maintain the phenotypes of PCOS mice [23] and were fed the classic KD (Fig. 1A). The treatments with ketogenic diet or the control diet were continued for 3 weeks. The mice were then sacrificed when they were 9 weeks old.

The blood ketone levels were similar among the three groups of mice after modeling and were significantly higher in letro + KD mice than in ctrl and letro mice 2 and 3 weeks after KD treatment (Fig. 1B). The body weight of letro + KD mice was markedly higher than that of ctrl mice at the end of the modeling (Fig. 1C) and significantly reduced at the end of KD treatment compared with letro mice (Fig. 1C, D). However, the letro + KD mice did not exhibit obvious improvements in glucose tolerance or insulin tolerance, as indicated by data from oral glucose tolerance test (OGTT) and insulin tolerance test (ITT) experiments (Supplemental Fig. 2A-D). The fasting and random blood glucose levels in letro + KD mice were significantly lower than in letro mice, which may be attributed to the shift in energy metabolism substrates (Supplemental Figs. 2E, F).

KD improves the ovarian function of letrozole-induced PCOS mice

To investigate the effect of the KD on the reproductive phenotype of the letro mice, we measured the serum testosterone levels of the animals. Serum testosterone (T) levels of the letro mice and letro + KD mice were markedly higher than in the ctrl animals, whereas there was no significant difference between the letro mice and letro + KD mice (Fig. 1E).

Meanwhile, the estrous cycles of the mice were monitored for 7 days during the 3-week treatment. The results

Table 1 Statistics of estrous cycle in the three groups of mice

	Number of mice with normal estrous cycle (n1/n2)	Percentage of improvement
ctrl	12/12	N/A
letro	0/12	0%
letro + KD	5/12	41.67%

n1: The number of mice with normal estrous cycle

n2: The total number of mice

N/A: No disturbance in estrous cycles

showed that control mice exhibited normal estrous cycles and letrozole-induced PCOS mice still showed disrupted estrous cycles. In contrast, the estrous cycles of 41.67% letro + KD mice were normal (Fig. 1F and Table 1), suggesting that the KD improved ovarian function in some letrozole-induced PCOS mice.

The ovarian sections were performed with H&E staining (Fig. 1G) and the numbers of ovarian cysts, corpora luteum, and follicles at all stages were counted. As shown in Fig. 1G and H, KD treatment did not reduce the number of ovarian cysts or corpora luteum in the letro + KD mice compared with letro mice, but the number of the follicles at all stages were significantly improved in the letro + KD mice compared with letro mice. Additionally, although the number of the ovarian cysts was not decreased in letro + KD mice compared with letro animals, the cyst area in letro + KD mouse ovarian section appeared smaller than that in letro mice, as shown in Fig. 1G. We thus calculated the percentage of the cyst area to the total section area and found that the percentage of the cyst area was markedly decreased in letro + KD mice compared with letro mice (Fig. 1I). However, the percentage was still significantly higher than in control mice.

KD reduces apoptosis in the ovaries of letro + KD mice

Due to the morphology of follicles in the mouse ovaries, TUNEL staining was performed to examine apoptosis. The fluorescence intensity of granulosa cells was stronger in letro mice than in letro + KD mice and ctrl mice, indicating reduced granulosa cell apoptosis by KD treatment (Fig. 1J).

KD alleviates inflammation in the ovaries of letro + KD mice

Apoptosis of granulosa cells can be induced by a variety of factors, such as inflammation. We thus examined the mRNA expression of inflammatory cytokine IL-6 in mouse ovaries. The IL-6 mRNA level was significantly higher in the ovaries of letro mice than in ctrl mice and letro + KD mice (Fig. 1K). Likewise, the mRNA level of inflammatory cytokine tumor necrosis factor-α (TNF-α) was significantly increased in the ovaries of letro mice than in ctrl mice, but no marked difference was found between letro mice and letro + KD animals (Supplemental Fig. 2G). Moreover, IL-6 levels in mouse ovarian supernatants, which mainly contained follicular fluid, were also examined (Fig. 1J). The IL-6 levels were markedly up-regulated in the ovarian supernatants of letro mice compared with ctrl mice and were significantly lower in letro + KD mice than in letro mice. These data suggested that KD treatment decreased inflammation in letrozole-induced PCOS mouse ovaries.

Taken together, these results revealed that the KD alleviated reproductive dysfunction in letrozole-induced PCOS mice possibly by inhibiting inflammation and reducing apoptosis of granulosa cells.

High concentrations of testosterone (T) induce apoptosis of KGN cells

To investigate the mechanisms by which KD reduced ovarian apoptosis in letrozole-induced PCOS mice, T was used to stimulate KGN cells. A series of concentrations of T at 1, 5, and 10 μM, respectively, were used to stimulate KGN cells for 24 h. Results from cell viability experiments showed that T induced apoptosis of KGN cells in a dose-dependent manner (Supplemental Fig. 3A). In addition, time-course of the effect of T at 10 μM on cell viability from 0 to 48 h was performed, as shown in Supplemental Fig. 3B. Treatment of KGN cells with T at 10 μM for 24 h resulted in significant cell death and was thus used in later experiments.

BHB declines T-induced apoptosis of KGN cells

BHB is the most abundant ketone body in the body. In mice, KD treatment markedly raised the serum BHB levels. In our previous study, BHB effectively reduced DHEA-induced inflammation in KGN cells [16]. The mechanism, however, was not well explained. We thus used the combination of BHB and T to treat the cells to explore the mechanism by which KD alleviated apoptosis in PCOS mouse ovaries.

KGN cells treated with 10 μM T for 24 h had a significant decrease in cell viability and an increase in apoptosis compared with the control group, as detected by MTT and flow cytometry (Fig. 2A-C). The concentration of BHB at 5 mM was chosen according to our previous study [16]. As illustrated in Fig. 2A-C, treatment with BHB alone did not have apparent effect, whereas BHB significantly increased cell viability and decreased cell apoptosis of T-treated KGN cells. Moreover, we also examined the levels of intracellular Caspase-3 and cleaved Caspase-3. Data from Western blot showed that the ratio of cleaved Caspase-3 to Caspase-3 was significantly higher in KGN cells treated with T than in controls (Fig. 2D, E). The treatment of KGN cells with the

combination of T and BHB reduced the ratio of cleaved Caspase-3/Caspase-3 compared with T treatment alone. Collectively, these data indicated that T induced apoptosis of KGN cells, which could be reversed by BHB.

Apoptosis of granulosa cells is associated with mitochondrial damage

Multiple studies [24, 25] have elucidated the role of mitochondria in the initiation and regulation of cell apoptosis. Apoptotic signals are transmitted into mitochondria, inducing the release of factors such as cytochrome C (Cyto C), SMAC/DIABLO, HTRA2/OMI, and ENDOG, followed by cell apoptosis through both caspase-dependent and independent pathways [24].

To verify whether mitochondria were involved in T-induced apoptosis of KGN cells, we examined the level of cytochrome C in the cellular cytoplasm without the component of mitochondria. The purity of extracted cellular cytoplasm without mitochondria was confirmed in Supplemental Fig. 4 with Cox4 as the marker of mitochondria. The release of cytochrome C from mitochondria is considered as one of the 'triggers' of the caspase cascade reaction [26]. Results showed a significant increase of cytochrome C in the cytoplasm of T-treated KGN cells, as compared with controls (Fig. 2F, G, Supplemental Fig. 4). The addition of BHB markedly inhibited T-induced cytoplasmic cytochrome C expression.

Moreover, the mitochondrial membrane potential was detected. JC-1 is a fluorescent probe widely used to detect mitochondrial membrane potential. Changes in the membrane potential are presumed to be associated with the opening of the mitochondrial permeability transition pore (mPTP), allowing the passage of ions and small molecules. As shown in Fig. 2H, I, KGN cells treated with T exhibited increased mitochondrial membrane permeability, which was significantly reduced by BHB. Adenosine triphosphate (ATP) production was measured as well. T treatment markedly reduced ATP production in KGN cells, which was improved by BHB (Fig. 2J).

Mitochondria are one of the main sources of cellular ROS. Mitochondrial ROS are produced by the leakage of electrons to form the superoxide at complex I and complex III in the electron transport chain [27]. Compared with the controls, T significantly increased intracellular ROS production in KGN cells treated with T (Fig. 2K, L). In contrast, ROS levels were markedly lower in cells treated with T + BHB than in cells treated with T alone. To further investigate the functional changes of mitochondria, the expression of mitochondrial DNA (mtDNA) was also measured. The cellular cytoplasm components without mitochondria were prepared as mentioned above. Real-time PCR was performed to evaluate the mtDNA copy number in the cytoplasm of KGN cells treated with vehicle (ctrl), T, BHB, or T + BHB. The results showed that T treatment increased the mtDNA content in the cytoplasm compared with ctrl, which was reduced by BHB (Fig. 2M).

Taken together, these results revealed that T caused granulosa cell apoptosis possibly by damaging mitochondria, which could be alleviated by BHB.

T activates cyclic GMP-AMP synthase (cGAS)-signaling effector stimulator of interferon genes (STING) pathway

Cyclic GMP-AMP synthase (cGAS) is the DNA sensor discovered in 2013. It is considered as a second messenger that functions by regulating its downstream molecule STING. It has been reported that the cGAS-STING pathway is closely associated with inflammation [28–31]. As we showed above, T induced the release of mtDNA into the cytoplasm. We thus detected the expression of cGAS and STING in KGN cells treated with vehicle (ctrl), T, BHB, or T + BHB. As shown in Fig. 3A, B, T treatment significantly increased the mRNA expression of cGAS, but not STING. The protein levels of both cGAS and STING were markedly up-regulated by T compared with ctrl (Fig. 3C-E). Treatment with BHB alone did not affect the expression of cGAS or STING compared with ctrl. The co-treatment of T and BHB, however, decreased cGAS and STING protein levels compared with T.

(See figure on next page.)

Fig. 2 Testosterone (T) induces apoptosis and mitochondrial damage in KGN cells, which were partially or in whole improved by BHB KGN cells were treated with T (0, 10 μM), BHB (5 mM), or the combination of T and BHB for 24 h. **A** Cell viability measured by MTT. $n = 6$ per group. **B** The percentage of cell apoptosis was measured by flow cytometry. **C** Statistical analysis of flow cytometry results. $n = 3$ per group. **D**, **E** Western blot analysis and densitometry quantification of Caspase-3 and Cleaved Caspase-3 in KGN cells. $n = 6$ per group. **F**, **G** Western blot analysis and densitometry quantification of cytochrome C (Cyto C) in the cytoplasm without mitochondria of KGN cells. β-actin was used as an internal control. $n = 6$ per group. **H** The mitochondrial membrane potential (ΔΨm) was determined by JC-1. Representative JC-1 staining of KGN cells from each group. Scale bar = 25 μm. **I** The ratios of JC-1 aggregate/monomer were analyzed by the Image J program. $n = 3$ per group. **J** Normalized ATP production of the cells. $n = 6$ per group. **K** Representative fluorescence micrographs of intracellular ROS in KGN cells. Scale bar = 25 μm. **L** The relative intensity of fluorescence of intracellular ROS was analyzed by the Image J program. Scale bar = 200 μm. $n = 6$ per group. **M** The relative ratio of mitochondrial DNA (ND1) to nuclear DNA (SLCO2B1) number. $n = 6$ per group. Data are presented as mean ± SEM. *, $P < 0.05$ *vs* ctrl, **, $P < 0.01$ *vs* ctrl, #, $P < 0.05$, ##, $P < 0.01$

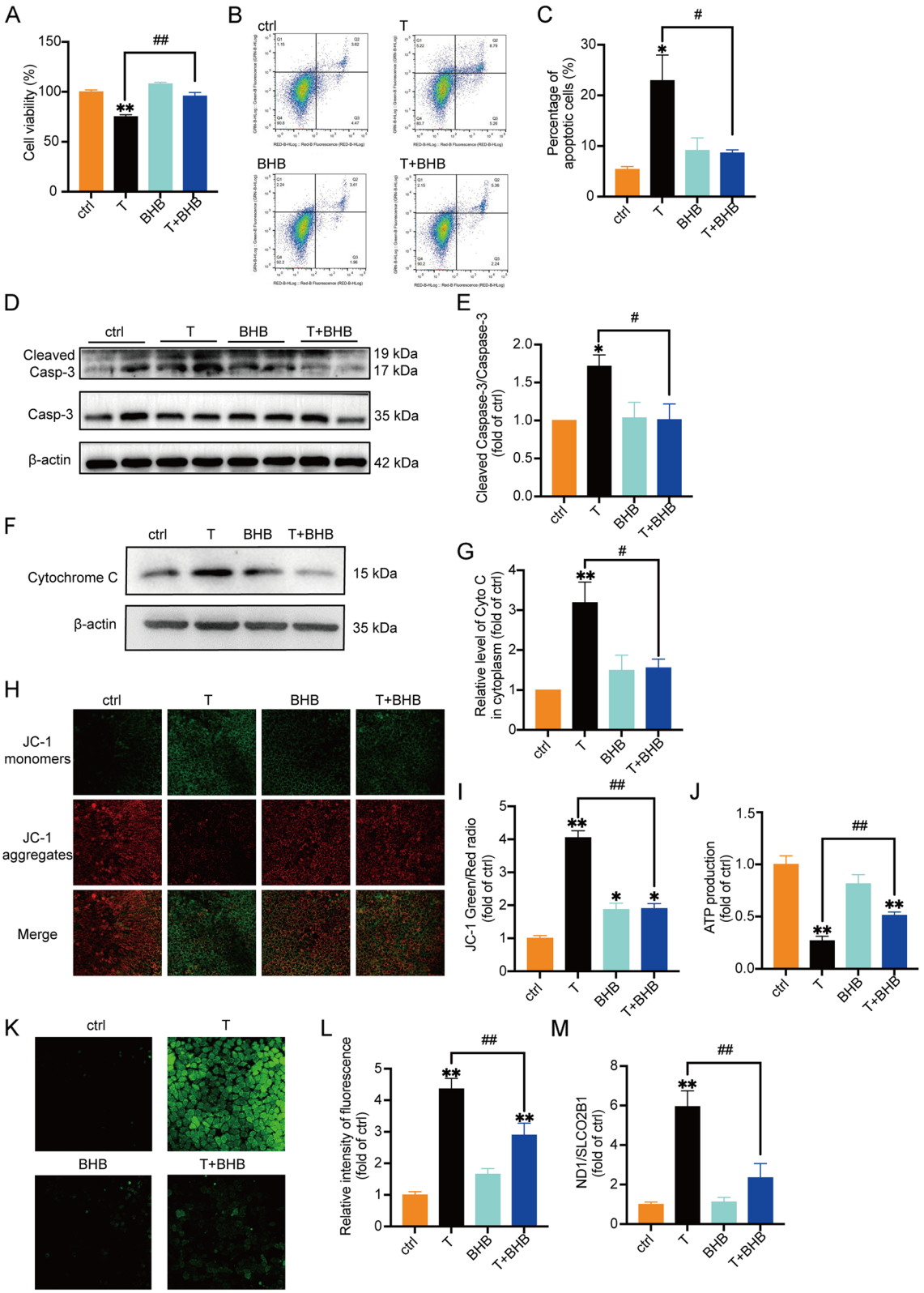

Fig. 2 (See legend on previous page.)

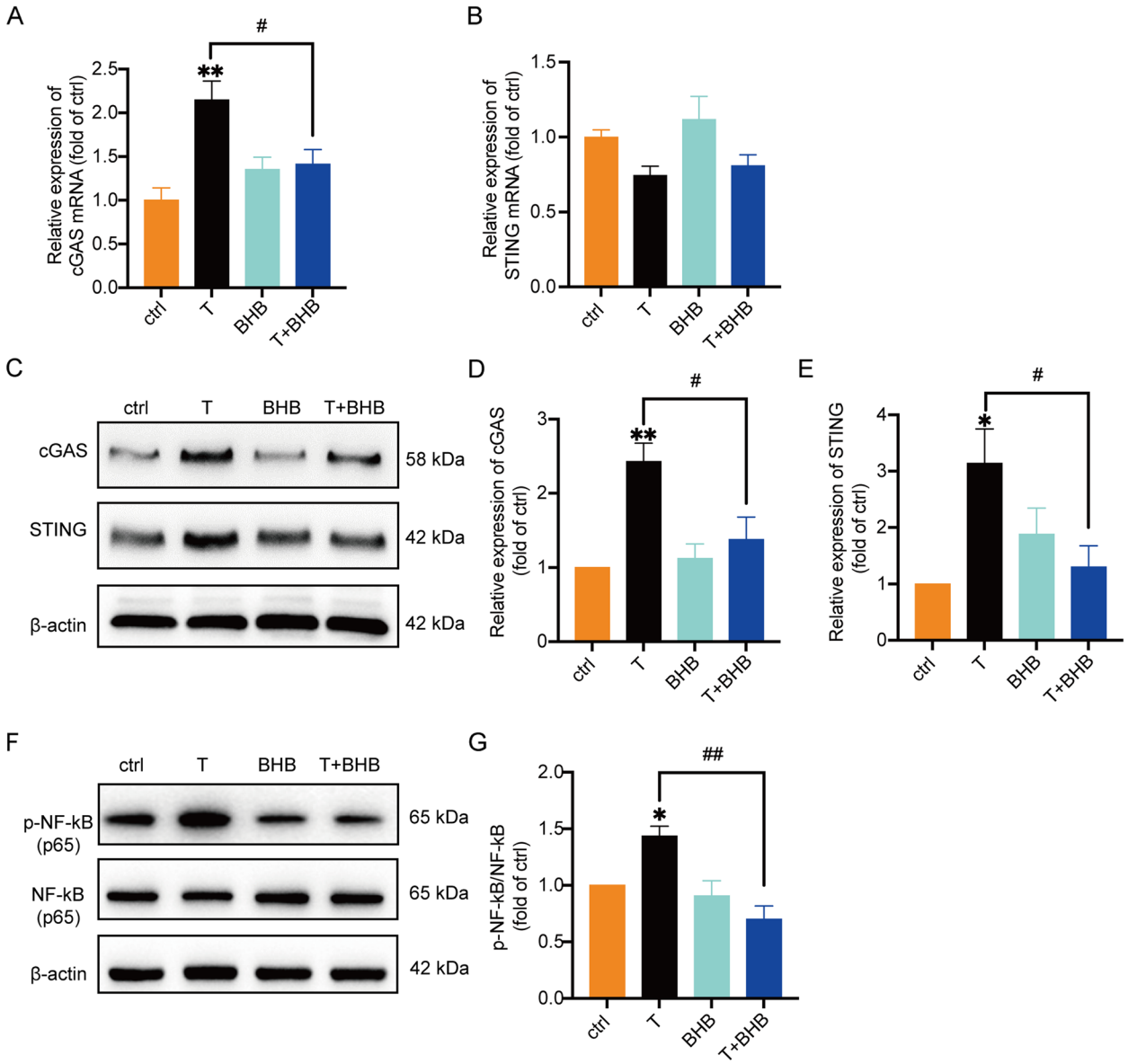

Fig. 3 T induces the activation of cGAS-STING signaling pathway, which can be partially decreased by BHB KGN cells treated with T (0, 10 μM), BHB (5 mM), or T + BHB for 24 h. **A** The relative mRNA expression of cGAS in the cells. $n = 8$ per group. **B** The relative mRNA expression levels of STING in the cells. $n = 6$ per group. **C-E** Western blot analysis and densitometry quantification of cGAS and STING in KGN cells. β-actin was used as an internal control. $n = 6$ per group. **F**, **G** Western blot analysis and densitometry quantification of NF-κB (p65) and phosphorylated NF-κB (p65) in the cells. $n = 6$ per group. Data are presented as mean ± SEM. *, $P < 0.05$ *vs* ctrl, **, $P < 0.01$ *vs* ctrl, #, $P < 0.05$, ##, $P < 0.01$

Activation of nuclear factor κB (NF-κB) is the downstream molecule of cGAS-STING pathway. As expected, T treatment significantly induced the phosphorylation of NF-κB (Fig. 3F, G), further confirming the activation of the cGAS-STING pathway induced by T. The cells treated with T + BHB exhibited a significantly lower ratio of p-NF-κB to NF-κB compared with T-treated cells. Collectively, a high concentration of T resulted in mitochondrial damage. The resulting release of mtDNA into the cytoplasm activated cGAS-STING pathway and the downstream molecule NF-κB, leading to inflammation in KGN cells.

T reduces cell viability and induces inflammation in KGN cells via cGAS-STING pathway

To address the role of cGAS-STING pathway in T-induced granulosa cell dysfunction, small interfering RNA (siRNA)-cGAS and a STING inhibitor C176

were used in the experiments. Three sequences of siRNA-cGAS numbered 1 to 3 were designed and transfected into KGN cells, respectively. The knockdown efficiency was checked. According to the mRNA and protein expression of cGAS (Supplemental Figs. 5A-B), siRNA-cGAS 3 was selected and used in the subsequent experiments. We then examined the effect of cGAS knockdown on cell viability, the expression of cGAS, STING, p-NF-κB and NF-κB in T-treated KGN cells. No apparent difference was observed between ctrl (only vehicle) and the negative control of siRNA-cGAS (nc) on cell viability (Fig. 4A). The knockdown of cGAS with siRNA-cGAS significantly elevated cell viability, reduced the expression of cGAS and STING, and decreased the ratio of p-NF-κB/NF-κB in T-treated cells compared with T treatment alone (Fig. 4A-E), which was similar to the effects of T + BHB. We then utilized a STING inhibitor C176 to further validate the role of STING in this process. The results showed that cell viability was markedly increased (Fig. 4F) and cell apoptosis was decreased (Fig. 4G) in T + C176 cells compared with cells treated with T alone. In addition, treatment with T + C176 significantly decreased the expression of cGAS, STING and the ratio of p-NF-κB to NF-κB (Fig. 4H-K). Taken together, these data suggested that the cGAS-STING pathway played an important role in T-induced granulosa cell damage. Blocking the cGAS-STING signaling pathway exhibited effects similar to BHB.

The cGAS-STING pathway plays a critical role in T-induced inflammation and cell apoptosis in KGN cells

Phosphorylation of p65, a member of NF-κB family, indicates the activation of NF-κB cascade, which is related to the promoted production of inflammatory factors such as IL-6 [32]. We thus measured IL-6 levels in culture medium and the cells treated with vehicle (ctrl), T, BHB, and T + BHB, respectively. Results from real-time PCR and ELISA showed that the levels of IL-6 were significantly higher in KGN cells treated with T than ctrl (Fig. 5A, B). BHB treatment alone did not apparently affect IL-6 synthesis or release. The combination of T + BHB, however, markedly reduced IL-6 levels in the cells and culture medium compared with T. Additionally, IL-6 synthesis and release in KGN cells treated with T + BHB were significantly higher than in ctrl, suggesting that BHB only partially reversed T-induced inflammation.

Since NF-κB is one downstream target of cGAS-STING pathway, we then assessed IL-6 levels after blocking cGAS or STING signaling. Transfection of siRNA-cGAS or the addition of C176, the STING inhibitor, significantly decreased T-induced IL-6 production and release, as illustrated in Fig. 5C-F. In addition, cell apoptosis that was at least partially triggered by T-induced inflammation, was down-regulated when the expression of cGAS or STING was decreased, as demonstrated by the ratio of cleaved Caspase-3/Caspase-3 (Fig. 5G-J). There was no apparent difference in IL-6 mRNA expression and release, or cell apoptosis between T + BHB and T + siRNA-cGAS, or T + BHB and T + C176 treatments (Fig. 5C-J).

Taken together, these results demonstrated that the cGAS-STING pathway plays an important role in T-induced inflammation and cell apoptosis in KGN cells. BHB reversed part of the T-induced cell damage possibly through cGAS-STING pathway.

Increased cGAS-STING signaling in letrozole-induced PCOS mouse ovaries is reduced by KD treatment

To verify the activation of the cGAS-STING signaling pathway in letrozole-induced PCOS mice, immunohistochemistry was performed to detect the expression of cGAS and STING in mouse ovaries. Results from immunohistochemical staining demonstrated the increased expression of cGAS and STING in the ovaries of letro mice, especially in granulosa cells (Fig. 6A-D). In contrast, the expression of cGAS and STING was decreased in the ovaries of letro + KD mice compared with letro animals. These data confirmed that improvement in the ovaries of letro + KD mice was at least in part through the cGAS-STING pathway.

Discussion

In this study, we found that hyperandrogenemia caused mitochondrial damage in granulosa cells under the condition of PCOS, which led to the leakage of cytochrome

(See figure on next page.)

Fig. 4 T reduces cell viability and induces inflammation in KGN cells via cGAS-STING pathway. **A** Cell viability measured by MTT. KGN cells were treated with the vehicle (ctrl), scrambled non-silencing RNA (nc), T (10 μM), T + BHB (5 mM), siRNA-cGAS,or T + siRNA-cGAS. $n = 6$ per group. **B-E** Western blot analysis and densitometry quantification of cGAS, STING, NF-κB (p65), and phosphorylated NF-κB (p65) in KGN cells treated as described as above. $n = 8$ per group for detection of cGAS and STING. $n = 6$ per group for detection of NF-κB (p65) and p-NF-κB (p65). **F** Cell viability measured by MTT. KGN cells were treated with the vehicle (ctrl), T (10 μM), T + BHB (5 mM), C176 (1 μM) and T + C176. $n = 6$ per group. **G** The percentage of apoptosis measured by flow cytometry. **H**–**K** Western blot analysis and densitometry quantification of cGAS, STING, NF-κB (p65), and phosphorylated NF-κB (p65) in KGN cells. $n = 6$ per group. Data are presented as mean ± SEM. *, $P < 0.05$ *vs* nc or ctrl, **, $P < 0.01$ *vs* nc or ctrl, #, $P < 0.05$, ##, $P < 0.01$

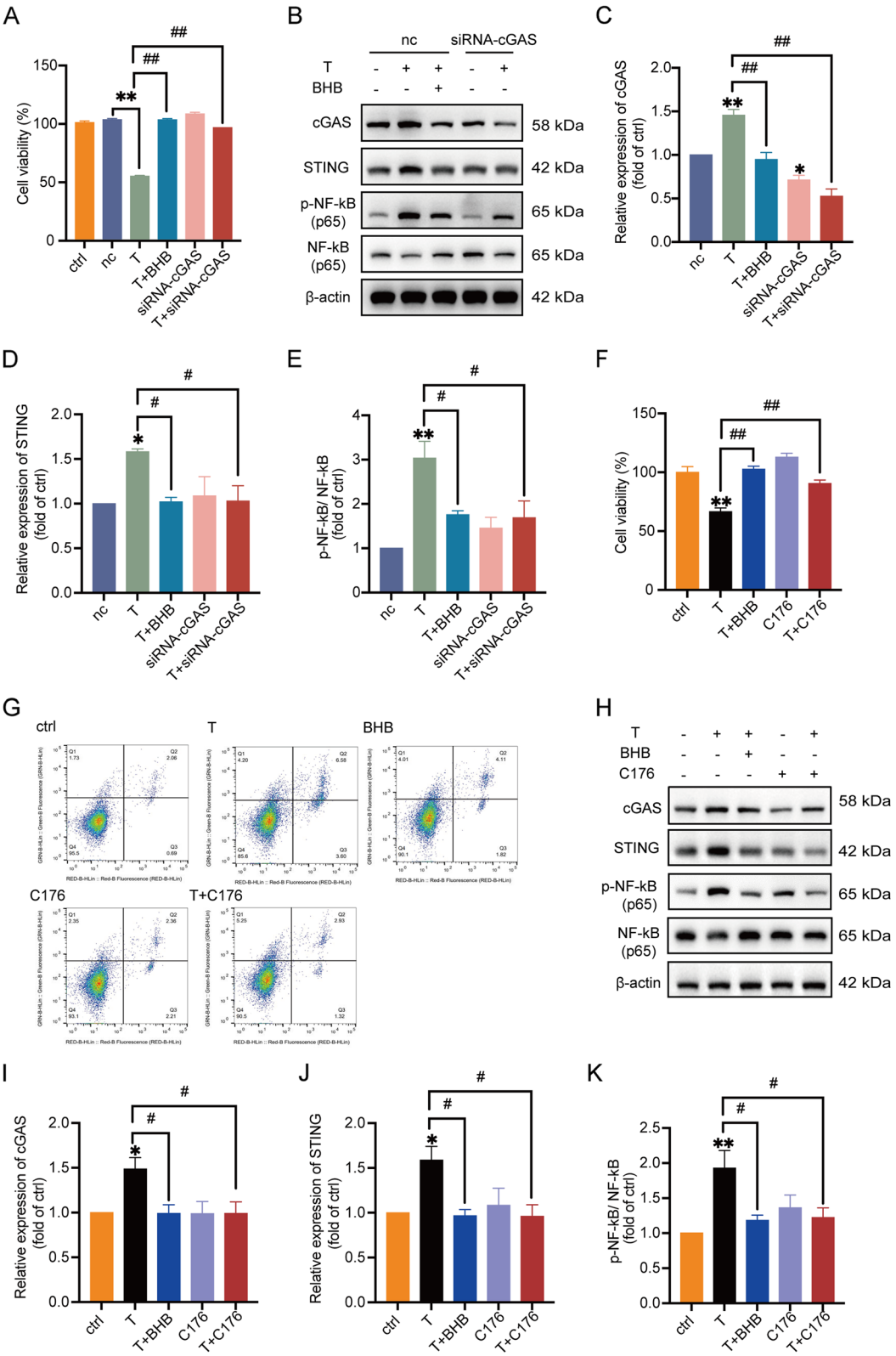

Fig. 4 (See legend on previous page.)

C and mtDNA from the mitochondria to the cytosol. It has been confirmed that cytochrome C is a key molecule leading to the caspase-related apoptosis [26]. In addition, the released mtDNA activated the cGAS-STING pathway followed by the phosphorylation of NF-κB. Cellular inflammatory responses were thus triggered. Inflammation and cytochrome C-induced caspase cascade together resulted in granulosa cell apoptosis. The KD treatment did not reduce plasma androgen levels in letrozole-induced PCOS mice, but it significantly improved reproductive phenotypes of the mice. These data suggested that the KD products in vivo inhibited the downstream signaling of androgens, instead of directly affecting the levels of androgens. Indeed, BHB, the main product of the KD, protected granulosa cells from hyperandrogenemia-induced mitochondrial damage and apoptosis. These findings are summarized in Fig. 7.

Since 2016, reports of KD treatment for PCOS have gradually increased. The primary physiological significance of ketone bodies is as an alternative energy source during fasting, but it is noteworthy that ketones also possess signaling properties [33]. Recent observations underscore the notion that ketone bodies play multiple signaling roles, such as modulating inflammation and oxidative stress.

Many studies have shown that ketone bodies may have therapeutic effects on neurodegenerative diseases by improving mitochondrial function [34, 35]. In PCOS animal models, the quantity and quality of mitochondria have also been evaluated. Jiang and colleagues [36] reported the presence of damaged mitochondria and fragmented mtDNA in the ovaries of a letrozole + HFD-induced PCOS rat model. Moreover, ATP levels were decreased in ovaries of PCOS rat models, indicating mitochondrial damage [37]. Likewise, we have also found mitochondrial dysfunction with reduced ATP levels and changed mitochondrial membrane potential in the present work, which is consistent with other studies [36–38]. However, the underlying mechanisms of mitochondrial damage in PCOS ovaries have not been revealed.

The leakage of mtDNA into the cellular cytosol is regarded as a danger-associated molecular pattern (DAMP) to trigger NF-κB-induced immune responses [28] under pathophysiologic conditions such as odontoblast inflammation [29], diabetic kidney disease [22] and liver sterile inflammation [30, 31]. Therefore, the mtDNA-induced cGAS-STING pathway seems to be a common pathway for chronic inflammation. PCOS is considered to be in a state of low-grade chronic inflammation. Particularly, local ovarian inflammation is generally not caused by pathogen infections. The role of cGAS-STING pathway in PCOS, however, has never been reported. In the present work, for the first time, our findings proved that high levels of T induced mtDNA leakage and thus activated cGAS-STING pathway. The cGAS-STING signaling pathway is a major effector of cellular sensing that responds to the presence of abnormal cytoplasmic double-stranded DNA (dsDNA). In addition to the release of exogenous DNA caused by pathogen invasion and replication, factors such as mitochondrial damage and genomic instability can also lead to abnormal leakage of endogenous dsDNA in the organism, which is then recognized by the DNA receptor cGAS, leading to the activation of the cGAS-STING pathway. The mitochondrial damage caused by high levels of androgens may be a key factor in the occurrence of ovarian sterile inflammation in PCOS.

The cGAS-STING signaling pathway is typically followed by the activation of NF-κB. After activation by STING, TANK-binding kinase 1 (TBK1) and its homolog IκB kinase epsilon (IKKε) can lead to activation of the IKK complex, which then activates the transcription factor NF-κB [39]. Thereafter, a prominent pro-inflammatory cytokine response is induced. Although a controlled immune response is beneficial, it can become detrimental when the response is too intense or the inflammatory process persists for an extended period of time. Key pro-inflammatory cytokines, including IL-1, IL-6, IL-18, IFN-γ, and TNF-α, are implicated in diseases such as epilepsy [40]. Excessive production and release of these pro-inflammatory cytokines are believed to have local and systemic cytotoxic effects. Molecular mechanisms include but are not limited to promoting chemotaxis of neutrophils and other immune cells, activating Toll-like

(See figure on next page.)

Fig. 5 The cGAS-STING pathway plays a critical role in T-induced inflammation and cell apoptosis in KGN cells. **A** The mRNA expression of IL-6 in KGN cells treated with T (0, 10 μM), BHB (5 mM), or T + BHB for 24 h. $n = 6$ per group. **B** The relative levels of IL-6 in the culture medium of KGN cells treated as above. $n = 6$ per group. **C** The relative mRNA expression of IL-6 in KGN cells treated with scrambled non-silencing RNA (nc), T (10 μM), T + BHB (5 mM), siRNA-cGAS, or T + siRNA-cGAS. $n = 6$ per group. **D** The relative levels of IL-6 in the culture medium of KGN cells. $n = 6$ per group. **E** The relative mRNA expression of IL-6 in KGN cells treated with the vehicle (ctrl), T (10 μM), T + BHB (5 mM), C176 (1 μM) and T + C176. $n = 6$ per group. **F** The relative levels of IL-6 in the culture medium of KGN cells. $n = 6$ per group. **G**, **H** Western blot analysis and densitometry quantification of Caspase-3 and Cleaved Caspase-3 in KGN cells. $n = 5$ per group. **I**, **J** Western blot analysis and densitometry quantification of Caspase-3 and Cleaved Caspase-3 in KGN cells. $n = 6$ per group. Data are presented as mean ± SEM. *, $P < 0.05$ *vs* nc or ctrl, **, $P < 0.01$ *vs* nc or ctrl, #, $P < 0.05$, ##, $P < 0.01$

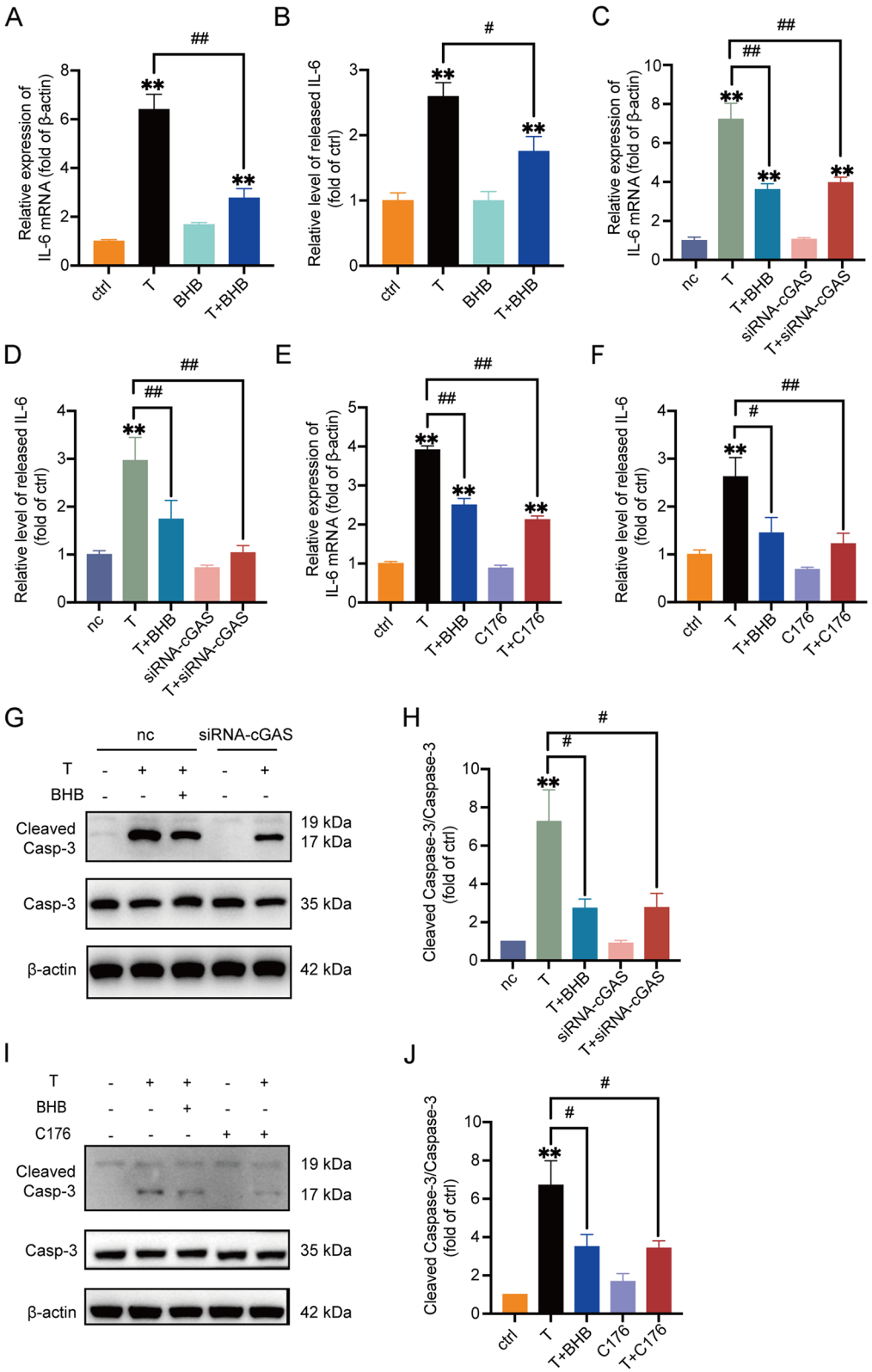

Fig. 5 (See legend on previous page.)

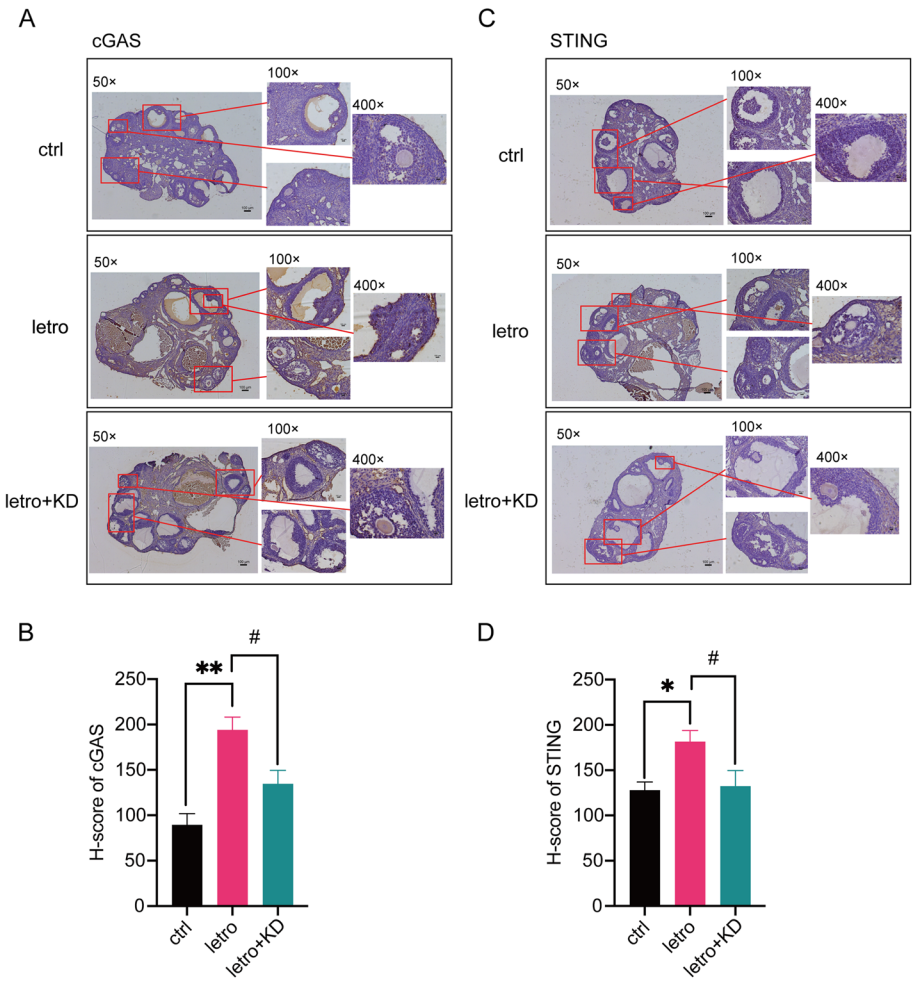

Fig. 6 cGAS-STING signaling in letrozole-induced PCOS mouse ovaries is reduced by KD treatment. **A** Representative immunohistochemistry staining for cGAS of ovarian sections of one mouse from each group. Scale bar = 100 μm. **B** H-score of the cGAS immunoreactivity in the ovaries. $n = 9$ per group. **C** Representative immunohistochemistry staining for STING of ovarian sections of one mouse from each group. Scale bar = 100 μm. **D** H-score of the STING immunoreactivity in the ovaries. $n = 9$ per group. Data are presented as mean ± SEM. *, $P < 0.05$ vs ctrl, **, $P < 0.01$ vs ctrl, #, $P < 0.05$, ##, $P < 0.01$

receptors and Th1 signaling pathway, and so on. However, the specific mechanism by which STING activates the NF-κB signaling pathway remains controversial, primarily regarding whether the phosphorylation of IKKβ by TBK1 is essential in this process [40, 41]. In the present work, we demonstrated the activation of NF-κB by cGAS-STING signaling pathway in granulosa cells treated with T, which is associated with increased apoptosis of these cells in PCOS. NF-κB can directly activate the IL-6/STAT3 pathway and so the expression of IL-6 reflects the activation status of NF-κB [42]. Consistent with NF-κB activation, we found that IL-6 mRNA expression was markedly up-regulated in PCOS mouse ovaries and the KD treatment significantly attenuated IL-6 levels. TNF-α is mainly secreted by macrophages [43]. Results from in vivo experiments showed that KD treatment did not affect TNF-α expression raised in PCOS mouse ovaries, suggesting that KD or BHB did not inhibit inflammation caused by ovarian macrophages. These data also implied that granulosa cells and macrophages induced inflammation through differential pathways.

The significant therapeutic effect of KD in obese women with PCOS has been confirmed in the clinic [4, 13–15]. However, there is a lack of adequate data to demonstrate the long-term safety of KD administration. Restrictive ketogenic diets used for epilepsy can cause fatigue, headache, nausea, constipation, hypoglycemia, and acidosis, especially within the first few days to weeks

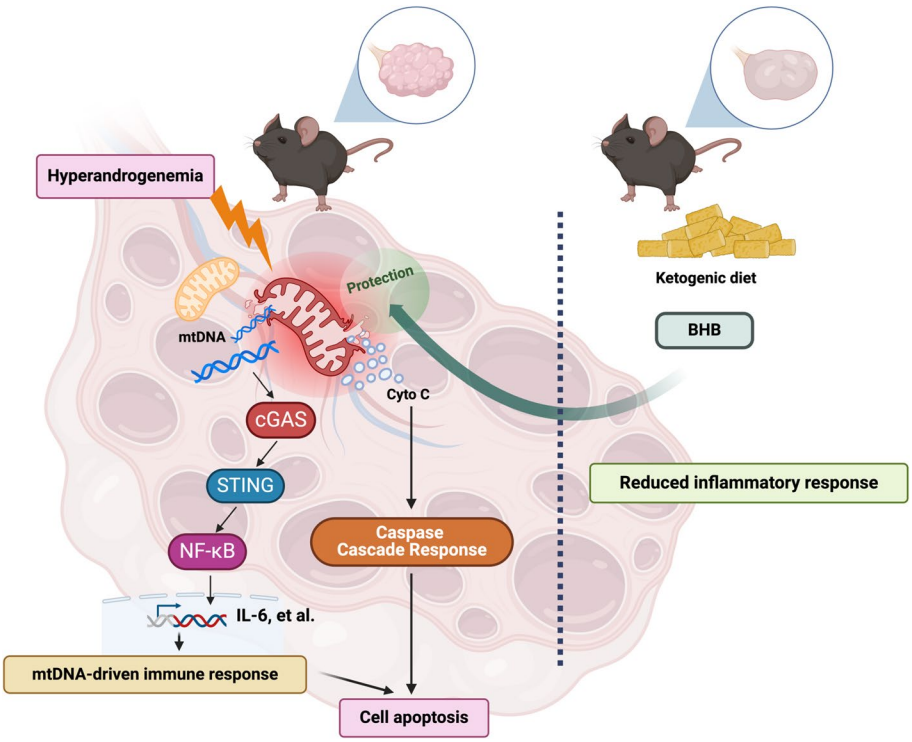

Fig. 7 Summary of the findings BHB, the main active product of KD, protects granulosa cells from mitochondrial damage and thus inhibits mtDNA-driven inflammation through the cGAS-STING-NF-κB pathway, leading to the decreased apoptosis of ovarian granulosa cells in PCOS

of treatment. Dehydration, hepatitis, pancreatitis, hypertriglyceridemia, hyperuricemia, hypercholesterolemia, hypomagnesemia, and hyponatremia can also occur [44]. The expected efficacy has extremely relied on the persistence and daily guidance from clinicians and self-administration of patients.

In summary, we have shown that KD played beneficial effects on reproductive phenotype of letrozole-induced PCOS mice in the present work. For the first time, our data unveiled that T induced granulosa cell damage via impairing mitochondria, which subsequently activated caspase cascade and the cGAS-STING-NF-κB signaling pathway, leading to cell apoptosis. BHB, the main product of KD, partially reversed T-induced granulosa cell damage by protecting mitochondria. There are several limitations in our study. One limitation lies in that the maximum duration we treated mice with KD was 3 weeks. We have no idea of the long-term safety of KD. Another is that we do not know why KD reduced the body weight of all the mice but only worked on some mice with regard to the improvement of reproductive phenotypes. Further research is needed to provide more evidence and mechanisms of KD therapy in PCOS.

Conclusion

The findings in our study indicate that mtDNA leakage is a crucial activator of the cGAS-STING-NF-κB pathway, contributing considerably to PCOS-associated inflammation in ovaries. The ketogenic diet offers a significant therapeutic approach to the ovarian dysfunction induced by hyperandrogenism by targeting mitochondrial damage and mtDNA leakage, thus alleviating the inflammation and apoptosis of granulosa cells. The mechanism we first reveal may be a new target for the future treatment of PCOS.

Abbreviations

PCOS	Polycystic ovary syndrome
KD	Ketogenic diet
BHB	β-Hydroxybutyrate
T	Testosterone
HA	Hyperandrogenism
OD	Ovulatory dysfunction
PCOM	Polycystic ovarian morphology
GI	Glycemic index
MD	Mediterranean diet
T2D	Type 2 diabetes
AcAc	Acetoacetate
Kbhb	β-Hydroxybutyrylation
DHEA	Dehydroepiandrosterone
IL-6	Interleukin-6
ROS	Reactive oxygen species

TNF-α	Tumor necrosis factor-α
Cyto C	Cytochrome C
mPTP	Mitochondrial permeability transition pore
ATP	Adenosine triphosphate
mtDNA	Mitochondrial DNA
cGAS	Cyclic GMP-AMP synthase
STING	Signaling effector stimulator of interferon genes
NF-κB	Nuclear factor κB
dsDNA	Double-stranded DNA

Supplementary Information

The online version contains supplementary material available at https://doi.org/10.1186/s12964-024-01939-6.

Supplementary Material 1: Supplemental Fig. 1. Verification of the establishment of a letrozole-induced PCOS mouse model (A) Serum testosterone level of the mice treated with letrozole or vehicle for 3 weeks. n = 6 per group. (B) Representative estrous cycle of one mouse from both groups from the second week. D, diestrus; M, metestrus; E, estrus; P, proestrus. (C) Representative H&E staining of ovarian sections of one mouse from both groups. Micrographs were taken at magnification × 50, scale bar = 100 μm. Data are presented as mean ± SEM. **, $P<0.01$ *vs* ctrl.

Supplementary Material 2: Supplemental Fig. 2. KD treatment does not improve glucose metabolism in PCOS mice The mice were treated with a control diet or KD for 3 weeks. (A) Oral glucose tolerance test (OGTT) curve (B) AUC of OGTT (C) Insulin tolerance test (ITT) curve (D) AUC of ITT (E) Fasting blood glucose levels of the mice. (F) Random blood glucose levels of the mice. (G) The mRNA expression of TNF-α in the ovaries of the mice. $n = 6$ per group. Data are presented as mean ± SEM. *, $P<0.05$ *vs* ctrl, **, $P<0.01$ *vs* ctrl, #, $P<0.05$.

Supplementary Material 3: Supplemental Fig. 3. T reduces KGN cell viability in a dose- and time-dependent manner (A) Cell viability measured by MTT. KGN cells were treated with different concentrations of T at 1, 5, and 10 μM, respectively, for 24 h. $n = 6$ per group. (B) Cell viability measured by MTT. KGN cells were treated with 10 μM T for a different time period. $n = 6$ per group. Data are presented as mean ± SEM. *, $P<0.05$ *vs* 0, **, $P<0.01$ *vs* 0, ##, $P<0.01$.

Supplementary Material 4: Supplemental Fig. 4. The purity verification of the extracted cellular cytoplasm without mitochondria Western blot analysis of Cox4 and β-actin using protein samples extracted from total cells and cytoplasm without mitochondria. Cox4 was used as a marker of mitochondrial protein, whereas β-actin was used as a maker of cytoplasmic protein.

Supplementary Material 5: Supplemental Fig. 5. Confirmation and selection of siRNA-cGAS sequences Three sequences of siRNA-cGAS were designed and transfected into KGN cells. (A) The mRNA expression of cGAS in KGN cells after siRNA-cGAS transfection for 36 h. $n = 6$ per group. (B) The protein expression of cGAS in KGN cells after siRNA-cGAS transfection for 48 h. Data are presented as mean ± SEM. **, $P<0.01$ *vs* nc.

Supplementary Material 6: Supplemental Table1. The primer sequences used for real-time PCR.

Supplementary Material 7: Supplemental Table 2. Three siRNA sequences for cGAS.

Supplementary Material 8.

Acknowledgments
Figures 1A and 7 were created with BioRender.com.

Authors' contributions
B.Z. and H.W. performed the experiments and analyzed the data. Q.Y. participated in data analysis processes. J.K., W. B., B.Z., and H.W. conceived the experimental designs. B.Z., H.W. and J.K. wrote the manuscript.

Funding
This research was supported by the National Natural Science Foundation of China (82171634, 31971068, and 81670733).

Data availability
No datasets were generated or analysed during the current study.

Declarations

Ethics approval consent to participate
All animal protocols were approved by the Animal Committee of Peking University Health Science Center in accordance with the Guide for the Care and Use of Laboratory Animals published by the US National Institutes of Health.

Consent for publication
Not applicable.

Competing interests
The authors declare no competing interests.

Author details
[1]Department of Physiology and Pathophysiology, School of Basic Medical Sciences, State Key Laboratory of Vascular Homeostasis and Remodeling, Peking University, Beijing, China. [2]Department of Obstetrics and Gynecology, Beijing Shijitan Hospital Affiliated to Capital Medical University, Beijing 100038, China. [3]Department of Physiology and Pathophysiology, School of Basic Medical Sciences, Peking University Health Science Center, No.38 Xueyuan Rd, Haidian District, Beijing 100191, China.

Received: 23 July 2024 Accepted: 10 November 2024
Published online: 27 November 2024

References

1. Teede HJ, Tay CT, Laven J, Dokras A, Moran LJ, Piltonen TT, Costello MF, Boivin J, Redman LM, Boyle JA, Norman RJ, Mousa A, Joham AE, International PCOS Network. Recommendations from the 2023 International evidence-based guideline for the assessment and management of polycystic ovary syndrome. Fertil Steril. 2023;120(4):767–93.
2. Azziz R, Carmina E, Chen Z, Dunaif A, Laven JS, Legro RS, Lizneva D, Natterson-Horowtiz B, Teede HJ, Yildiz BO. Polycystic ovary syndrome. Nat Rev Dis Primers. 2016;2:16057.
3. Barrea L, Arnone A, Annunziata G, Muscogiuri G, Laudisio D, Salzano C, Pugliese G, Colao A, Savastano S. Adherence to the Mediterranean diet, dietary patterns and body composition in women with Polycystic Ovary Syndrome (PCOS). Nutrients. 2019;11(10):2278.
4. Tsushima Y, Nachawi N, Pantalone KM, Griebeler ML, Alwahab UA. Ketogenic diet improves fertility in patients with polycystic ovary syndrome: a brief report. Front Nutr. 2024;11:1395977.
5. Wilder RM. High fat diets in epilepsy. Mayo Clin Bull. 1921;2:308.
6. Dyńka D, Kowalcze K, Paziewska A. The role of ketogenic diet in the treatment of neurological diseases. Nutrients. 2022;14(23):5003.
7. Li S, Du Y, Meireles C, Sharma K, Qi L, Castillo A, Wang J. Adherence to ketogenic diet in lifestyle interventions in adults with overweight or obesity and type 2 diabetes: a scoping review. Nutr Diabetes. 2023;13(1):16.
8. Barrea L, Verde L, Camajani E, Cernea S, Frias-Toral E, Lamabadusuriya D, Ceriani F, Savastano S, Colao A, Muscogiuri G. Ketogenic diet as medical prescription in women with Polycystic Ovary Syndrome (PCOS). Curr Nutr Rep. 2023;12(1):56–64.
9. Youm YH, Nguyen KY, Grant RW, Goldberg EL, Bodogai M, Kim D, D'Agostino D, Planavsky N, Lupfer C, Kanneganti TD, Kang S, Horvath TL, Fahmy TM, Crawford PA, Biragyn A, Alnemri E, Dixit VD. The ketone metabolite β-hydroxybutyrate blocks NLRP3 inflammasome-mediated inflammatory disease. Nat Med. 2015;21(3):263–9.
10. Lan Z, Chen A, Li L, Ye Y, Liang Q, Dong Q, Wang S, Fu M, Li Y, Liu X, Zhu Z, Ou JS, Qiu X, Lu L, Yan J. Downregulation of HDAC9 by the ketone metabolite β-hydroxybutyrate suppresses vascular calcification. J Pathol. 2022;258(3):213–26.

11. Trotta MC, Maisto R, Guida F, Boccella S, Luongo L, Balta C, D'Amico G, Herman H, Hermenean A, Bucolo C, D'Amico M. The activation of retinal HCA2 receptors by systemic beta-hydroxybutyrate inhibits diabetic retinal damage through reduction of endoplasmic reticulum stress and the NLRP3 inflammasome. PLoS One. 2019;14(1):e0211005.
12. Zhou T, Cheng X, He Y, Xie Y, Xu F, Xu Y, Huang W. Function and mechanism of histone β-hydroxybutyrylation in health and disease. Front Immunol. 2022;13:981285.
13. Paoli A, Mancin L, Giacona MC, Bianco A, Caprio M. Effects of a ketogenic diet in overweight women with polycystic ovary syndrome. J Transl Med. 2020;18(1):104.
14. Cincione RI, Losavio F, Ciolli F, Valenzano A, Cibelli G, Messina G, Polito R. Effects of mixed of a ketogenic diet in overweight and obese women with polycystic ovary syndrome. Int J Environ Res Public Health. 2021;18(23):12490.
15. Magagnini MC, Condorelli RA, Cimino L, Cannarella R, Aversa A, Calogero AE, La Vignera S. Does the ketogenic diet improve the quality of ovarian function in obese women? Nutrients. 2022;14(19):4147.
16. Liu S, Yao Q, Li X, Wu H, Sun C, Bai W, Kang J. Effects of a ketogenic diet on reproductive and metabolic phenotypes in mice with polycystic ovary syndrome. Biol Reprod. 2023;108(4):597–610.
17. Zhang X, Xiao H, Zhang X, Qiukai E, Gong X, Li T, Han Y, Ying X, Cherrington BD, Xu B, Liu X, Zhang X. Decreased microRNA-125b-5p disrupts follicle steroidogenesis through targeting PAK3/ERK1/2 signalling in mouse preantral follicles. Metabolism. 2020;107:154241.
18. Lai H, Jia X, Yu Q, Zhang C, Qiao J, Guan Y, Kang J. High-fat diet induces significant metabolic disorders in a mouse model of polycystic ovary syndrome. Biol Reprod. 2014;91(5):127.
19. Yang Y, Xiao M, Song Y, et al. H-score of 11β-hydroxylase and aldosterone synthase in the histopathological diagnosis of adrenocortical tumors. Endocrine. 2019;65(3):683–91.
20. He L, Ling L, Wei T, Wang Y, Xiong Z. Ginsenoside Rg1 improves fertility and reduces ovarian pathological damages in premature ovarian failure model of mice. Exp Biol Med (Maywood). 2017;242(7):683–91.
21. Yao Q, Zou X, Liu S, Wu H, Shen Q, Kang J. Oxidative Stress as a contributor to insulin resistance in the skeletal muscles of mice with polycystic ovary syndrome. Int J Mol Sci. 2022;23(19):11384.
22. Zang N, Cui C, Guo X, Song J, Hu H, Yang M, Xu M, Wang L, Hou X, He Q, Sun Z, Wang C, Chen L. cGAS-STING activation contributes to podocyte injury in diabetic kidney disease. iScience. 2022;25(10):105145.
23. Wu H, Zhao B, Yao Q, Kang J. Dehydroepiandrosterone-induced polycystic ovary syndrome mouse model requires continous treatments to maintain reproductive phenotypes. J Ovarian Res. 2023;16(1):207.
24. Yuan J, Ofengeim D. A guide to cell death pathways. Nat Rev Mol Cell Biol. 2024;25(5):379–95.
25. Li H, Wang X, Mu H, Mei Q, Liu Y, Min Z, Zhang L, Su P, Xiang W. Mir-484 contributes to diminished ovarian reserve by regulating granulosa cell function via YAP1-mediated mitochondrial function and apoptosis. Int J Biol Sci. 2022;18(3):1008–21.
26. Santucci R, Sinibaldi F, Cozza P, Polticelli F, Fiorucci L. Cytochrome c: an extreme multifunctional protein with a key role in cell fate. Int J Biol Macromol. 2019;136:1237–46.
27. Su L, Zhang J, Gomez H, Kellum JA, Peng Z. Mitochondria ROS and mitophagy in acute kidney injury. Autophagy. 2023;19(2):401–14.
28. Maekawa H, Inoue T, Ouchi H, Jao TM, Inoue R, Nishi H, Fujii R, Ishidate F, Tanaka T, Tanaka Y, Hirokawa N, Nangaku M, Inagi R. Mitochondrial damage causes inflammation via cGAS-STING signaling in acute kidney injury. Cell Rep. 2019;29(5):1261-1273.e6.
29. Zhou L, Zhang YF, Yang FH, Mao HQ, Chen Z, Zhang L. Mitochondrial DNA leakage induces odontoblast inflammation via the cGAS-STING pathway. Cell Commun Signal. 2021;19(1):58.
30. Yang NS, Zhong WJ, Sha HX, Zhang CY, Jin L, Duan JX, Xiong JB, You ZJ, Zhou Y, Guan CX. mtDNA-cGAS-STING axis-dependent NLRP3 inflammasome activation contributes to postoperative cognitive dysfunction induced by sevoflurane in mice. Int J Biol Sci. 2024;20(5):1927–46.
31. Zhong W, Rao Z, Xu J, Sun Y, Hu H, Wang P, Xia Y, Pan X, Tang W, Chen Z, Zhou H, Wang X. Defective mitophagy in aged macrophages promotes mitochondrial DNA cytosolic leakage to activate STING signaling during liver sterile inflammation. Aging Cell. 2022;21(6):e13622.
32. Yu H, Lin L, Zhang Z, Zhang H, Hu H. Targeting NF-κB pathway for the therapy of diseases: mechanism and clinical study. Signal Transduct Target Ther. 2020;5(1):209.
33. Newman JC, Verdin E. Ketone bodies as signaling metabolites. Trends Endocrinol Metab. 2014;25(1):42–52.
34. Maalouf M, Rho JM, Mattson MP. The neuroprotective properties of calorie restriction, the ketogenic diet, and ketone bodies. Brain Res Rev. 2009;59(2):293–315.
35. Lim S, Chesser AS, Grima JC, Rappold PM, Blum D, Przedborski S, Tieu K. D-β-hydroxybutyrate is protective in mouse models of Huntington's disease. PLoS One. 2011;6(9):e24620.
36. Jiang XL, Tai H, Xiao XS, Zhang SY, Cui SC, Qi SB, Hu DD, Zhang LN, Kuang JS, Meng XS, Li SM. Cangfudaotan decoction inhibits mitochondria-dependent apoptosis of granulosa cells in rats with polycystic ovarian syndrome. Front Endocrinol (Lausanne). 2022;13:962154.
37. Rabah HM, Mohamed DA, Mariah RA, Abd El-Khalik SR, Khattab HA, AbuoHashish NA, Abdelsattar AM, Raslan MA, Farghal EE, Eltokhy AK. Novel insights into the synergistic effects of selenium nanoparticles and metformin treatment of letrozole - induced polycystic ovarian syndrome: targeting PI3K/Akt signalling pathway, redox status and mitochondrial dysfunction in ovarian tissue. Redox Rep. 2023;28(1):2160569.
38. Wang F, Han J, Wang X, Liu Y, Zhang Z. Roles of HIF-1α/BNIP3 mediated mitophagy in mitochondrial dysfunction of letrozole-induced PCOS rats. J Mol Histol. 2022;53(5):833–42.
39. Balka KR, Louis C, Saunders TL, Smith AM, Calleja DJ, D'Silva DB, Moghaddas F, Tailler M, Lawlor KE, Zhan Y, Burns CJ, Wicks IP, Miner JJ, Kile BT, Masters SL, De Nardo D. TBK1 and IKKε act redundantly to mediate STING-induced NF-κB responses in myeloid cells. Cell Rep. 2020;31(1):107492.
40. Atabaki R, Khaleghzadeh-Ahangar H, Esmaeili N, Mohseni-Moghaddam P. Role of pyroptosis, a pro-inflammatory programmed cell death, in Epilepsy. Cell Mol Neurobiol. 2023;43(3):1049–59.
41. Zhang L, Wei X, Wang Z, Liu P, Hou Y, Xu Y, Su H, Koci MD, Yin H, Zhang C. NF-κB activation enhances STING signaling by altering microtubule-mediated STING trafficking. Cell Rep. 2023;42(3):112185.
42. Guo Q, Jin Y, Chen X, et al. NF-κB in biology and targeted therapy: new insights and translational implications. Signal Transduct Target Ther. 2024;9(1):53.
43. Van Loo G, Bertrand MJM. Death by TNF: a road to inflammation. Nat Rev Immunol. 2023;23(5):289–303.
44. Crosby L, Davis B, Joshi S, Jardine M, Paul J, Neola M, Barnard ND. Ketogenic diets and chronic disease: weighing the benefits against the risks. Front Nutr. 2021;8:702802.

Publisher's Note